Chapter 8
Calibration: Correction for the misalignment of the instruments optical axis

8.1 Introduction

The in-flight calibration of the scientific payload of *INTEGRAL* was a complex task which took place directly after launch, during the so-called commissioning phase. The commissioning phase lasted about two months and included the following: Transition to the operational orbit, instruments activations, optimization of the instruments configurations, performance and validation (PV) phase. During the PV phase, a set of observations were made on the Cygnus region, testing different dithering combinations. It was thus possible to start calibrating the instruments using the first scientific images produced by *INTEGRAL*. We started to work on the correction of the misalignment of the instruments optical axis, with these first data, but it took several iterations to finally complete the task in July 2003.

There are several reasons to this delay: The outgassing and cooling down of SPI was completed the 11th of November 2002, but it took nevertheless several more months to have enough statistics in the data to perform the necessary computations for this instrument. For IBIS, it was already possible to progress with the two sources detected during the PV phase (Cyg X-1 and Cyg X-3), but a new iteration using the Crab brought improved results. The Crab observation took place in February 2003, the source was not visible earlier by *INTEGRAL*.

A refined computation of the ISGRI alignment took place in June 2004 in order to take into account several significant changes which occurred in the analysis software in 2003-early 2004. The first is the distance mask-detector which has been precised and the second is a new point-spread function.

In the X-ray domain covered by JEM-X, the Crab Nebula is an extended source of $1'$ size which has a maximum not coincident with the pulsar position (offset of $10''$ to about $20''$ depending on the energy range; see Brandt et al. 2003a, see also Pelling et al. 1987). For JEM-X2, it was possible to use an observation of GRS 1915+105 to avoid this problem, but not for JEM-X1 which was put in dormant mode shortly after PV phase, due to the quick deterioration of the instrument caused by the dead anode problem (see Brandt et al. 2003b).

In the following, we first describe the misalignment problem and write down the equations necessary to make the different transformations. We describe the computations of the so-called "misalignment matrices" (see below) and give an overview of the performances. Finally, the published results are closing this chapter (Walter et al. 2003). The C++ code needed to perform these computations is added in annex C (see also under /home/isdc/favre/misalignment/* on the ISDC system).

8.2 The misalignment of an instrument optical axis

The misalignment of an instrument optical axis with respect to the spacecraft (hereafter S/C) optical axis, given by the star trackers, introduces systematic errors on the source coordinates determined by the analysis software (hereafter S/W; see Courvoisier et al. 2003). We will not elaborate on the possible causes of such a misalignment and just mention that part of it is already existing prior to launch, due to various mechanical constraints in the S/C structure (see e.g. the minutes of the FAR meeting, ESTEC, June 21st 2002). In addition, one expects than the launch itself has brought a part of misalignment, due to induced vibrations, passage from 1 g to 0 g, moisture release and outgassing, but also to the large temperature variations. Note that due to the structure of the S/C itself, it is more likely that we measure the misalignment of the star trackers with respect to the instruments. If this assumption is confirmed, the correction should be of roughly the same amplitude and direction for all instruments.

8.2.1 The six misalignment matrices

Once quantified, the problem can be corrected by including a little rotation in the analysis S/W, which in practice takes the form of an Euler matrix, called here the misalignment matrix. Due to the different spatial resolution of the *INTEGRAL* instruments, a different misalignment matrix is needed for each instrument. The six matrices for each of the six instruments (ISGRI, PICsIT, SPI, JEM-X1, JEM-X2, OMC) were thus computed using in-flight data from the PV and calibration phases, and stored in a specific location in the distributed S/W. They correct automatically the positions when the analysis S/W is run.

8.3 Definition of the problem, for one instrument i

8.3.1 Definition of the geometry

We shall work with the following three reference frames:

- Celestial EQUatorial frame J2000, $\vec{e_1}$, $\vec{e_2}$, $\vec{e_3}$ (hereafter EQU);
- Star Tracker frame, $\vec{x}$, $\vec{y}$, $\vec{z}$ (hereafter ST);
- INSTrument i frame, $\vec{x'}$, $\vec{y'}$, $\vec{z'}$ (hereafter INST).

These are illustrated in Fig. 8.1.

8.3.2 Spacecraft attitude

The $\vec{x}$ axis gives the pointing direction of the S/C which is derived from its attitude data. The S/C attitude can be defined in two ways: By the $\vec{x}$ and $\vec{z}$ axis, in the Equatorial (EQU) frame or by the $\vec{x}$ axis and position angle (illustrated in Fig. 8.3). We will use here the first possibility (one can convert position angle to $\vec{z}$ axis using the DAL3AUXcalcZAxis() tool within isdcroot when necessary; see DAL3AUX User Manual (2004)). We assume here that the star trackers

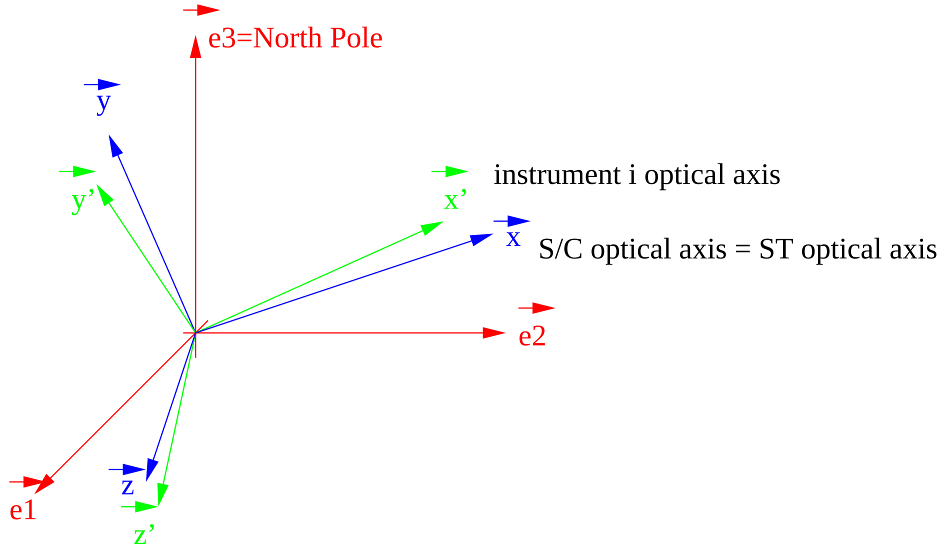

Figure *8.1: The three reference frames. In red: the Celestial EQUatorial frame $\vec{e_1}$, $\vec{e_2}$, $\vec{e_3}$ (EQU); in blue: the Star Tracker frame $\vec{x}$, $\vec{y}$, $\vec{z}$ (ST); in green: the INSTrument i frame $\vec{x'}$, $\vec{y'}$, $\vec{z'}$ (INST). All the basis are orthonormal. The detector plane is defined by $\vec{z'}$ and $\vec{y'}$.*

are not misaligned with respect to the overall S/C axis, i.e. the S/C optical axis is the ST $\vec{x}$ axis.

8.3.3 Instrument frame

The $\vec{x}$ and $\vec{x'}$ axis are located in the EQU frame through the angles ra_scx, dec_scx and ra_scx_INST, dec_scx_INST (Fig. 8.2).

The same names are used in the DAL3AUX S/W. The pointing direction of the instrument i in the EQU frame is often called the boresight of the instrument.

In a similar way, the $\vec{z}$ and $\vec{z'}$ axis are defined by ra_scz, dec_scz, ra_scz_INST, dec_scz_INST while the $\vec{y}$ and $\vec{y'}$ axis are found by taking the cross-products $\vec{y} = \vec{z} \wedge \vec{x}$ and $\vec{y'} = \vec{z'} \wedge \vec{x'}$.

The relation between the S/C pointing axis and the instrument i pointing axis in the EQU frame is made using a rotation matrix N:

$$\begin{pmatrix} Cos(dec\_scx\_INST)Cos(ra\_scx\_INST) \\ Cos(dec\_scx\_INST)Sin(ra\_scx\_INST) \\ Sin(dec\_scx\_INST) \end{pmatrix}_{EQU} = N \begin{pmatrix} Cos(dec\_scx)Cos(ra\_scx) \\ Cos(dec\_scx)Sin(ra\_scx) \\ Sin(dec\_scx) \end{pmatrix}_{EQU} \tag{8.1}$$

Note that since the basis are orthonormal, we have $N^{-1} = N^T$. The matrix N is not yet the misalignment matrix. N includes two components which must be disentangled: The first is the misalignment itself, which is a small rotation independent of the pointing direction of the S/C and the second is the rotation corresponding to the S/C attitude itself. The relation between these two components is described below (Sect. 8.4).

8.3.4 Method for the derivation of the misalignment matrix

The problem can be simply stated as follows. The unknowns are the nine components of the misalignment matrix, for the instrument i, given the S/C attitude and the discrepancy between the source position we measured with a "misaligned" instrument, and the true, catalog

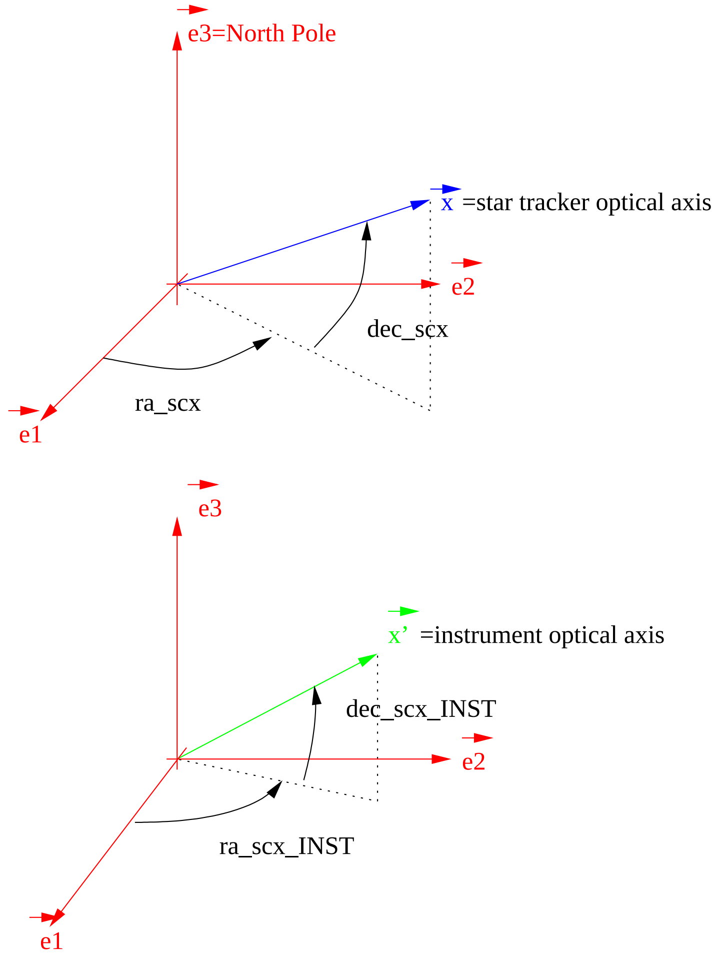

Figure *8.2: Top: definition of the S/C optical axis in the EQU frame. Bottom: definition of the instrument i optical axis in the EQU frame.*

position of the source. Prior to launch, the six matrices were set to unity. During PV phase, the six instruments were thus initially "misaligned".

We shall define the measured source position with two angles ra_src_{EQU}, dec_src_{EQU}, in the *EQU* frame (Fig. 8.3). These are thus affected by a systematic error and different from ra_src and dec_src which is found in the standard optical/X-ray catalogs, in the EQU frame.

The two vectors describing the same source in the EQU frame can be related using the rotation matrix N defined above:

$$\begin{pmatrix} source \\ j \\ measured \end{pmatrix}_{EQU} = N \begin{pmatrix} source \\ j \\ catalog \end{pmatrix}_{EQU} \tag{8.2}$$

Three sources are thus needed to deduce the nine elements of N through the three parameters describing the rotation, e.g. the three Euler angles. Deduction of (8.2) from (8.1) can be understood easily if we imagine that the S/C is exactly pointing on the particular source under study. In other words, if we correct the boresight, then all the sources will be found at

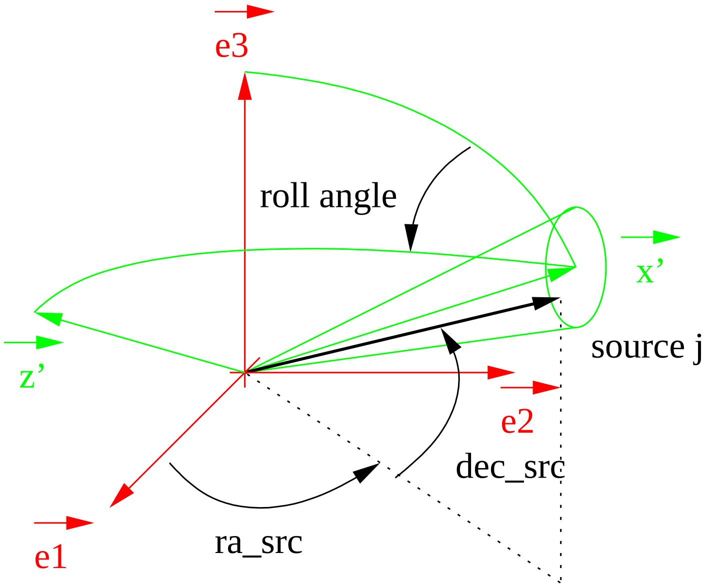

Figure *8.3: An example of a source in the FOV of instrument i. The instrument attitude is defined by the $\vec{x'}$ and $\vec{z'}$ axis, or in terms of $\vec{x'}$ axis and roll angle (this last representation is useful but does not bring more information).*

their correct locations.

This is the first part of the problem. We will show below that the previous description is only valid for a particular pointing. To fully understand and solve the problem, we need to go a step further and describe the full transformations between the three reference frames.

8.4 Frame transformations

The following two transformations are needed:

- EQU frame from/to ST frame;
- ST frame from/to INST frame.

8.4.1 Solution using Euler matrices

8.4.2 Reminder

Using linear algebra, a transformation matrix T from a frame B to a frame A is constructed by filling the matrix columns with images of the basis vectors of B in the frame A; $\left(\vec{B}_i\right)_A$ (see e.g. the textbook by Strang (1988)). We shall write $T\,()_B = ()_A$ for the transformation, where () is a vector in 3 dimensions.

8.4.3 ST to EQU

From the S/C attitude given by the star trackers, the following transformation matrix can be defined:

$$\begin{aligned} S^T &= \begin{pmatrix} \vec{x}_{EQU} & \vec{y}_{EQU} & \vec{z}_{EQU} \end{pmatrix} \\ &= \begin{pmatrix} Cos(dec\_scx)Cos(ra\_scx) & (\vec{z}\wedge\vec{x})_1 & Cos(dec\_scz)Cos(ra\_scz) \\ Cos(dec\_scx)Sin(ra\_scx) & (\vec{z}\wedge\vec{x})_2 & Cos(dec\_scz)Sin(ra\_scz) \\ Sin(dec\_scx) & (\vec{z}\wedge\vec{x})_3 & Sin(dec\_scz) \end{pmatrix} \end{aligned} \tag{8.3}$$

where S^T is the matrix transpose of S. Thus $S^T\,()_{ST} = ()_{EQU}$.

8.4.4 INST to ST

One cannot use the same idea for the instrument axis $\vec{x'}$, $\vec{y'}$, $\vec{z'}$, as this will result of a transformation INST to EQU (see also (8.1)). A more general rotation matrix is needed. A rotation in three dimensions is usually simply defined as a combination of three rotations about the basis vectors. In the very intuitive Cardan representation we discuss below, a rotation is made about each axis (roll: $\vec{x'}$, pitch: $\vec{y'}$, yaw: $\vec{z'}$), while in the standard Euler representation, two rotations are made about the $\vec{z'}$ axis. Note that in both cases, the second rotation is already made around rotated axis (see e.g. Arfken (1985), p.198, for more details on the standard Euler representation).

The rotation about the roll axis by α is given by:

$$\mathrm{roll}(\alpha) = \begin{pmatrix} 1 & 0 & 0 \\ 0 & Cos(\alpha) & -Sin(\alpha) \\ 0 & Sin(\alpha) & Cos(\alpha) \end{pmatrix} \tag{8.4}$$

the rotation about the pitch axis by β is given by:

$$\mathrm{pitch}(\beta) = \begin{pmatrix} Cos(\beta) & 0 & Sin(\beta) \\ 0 & 1 & 0 \\ -Sin(\beta) & 0 & Cos(\beta) \end{pmatrix} \tag{8.5}$$

and the rotation about the yaw axis by γ is given by:

$$\mathrm{yaw}(\gamma) = \begin{pmatrix} Cos(\gamma) & -Sin(\gamma) & 0 \\ Sin(\gamma) & Cos(\gamma) & 0 \\ 0 & 0 & 1 \end{pmatrix} \tag{8.6}$$

The final rotation INST to ST is the matrix product:

$$M(\alpha,\beta,\gamma) = \mathrm{yaw}(\gamma)\mathrm{pitch}(\beta)\mathrm{roll}(\alpha) = \tag{8.7}$$

$$\begin{pmatrix} Cos(\beta)Cos(\gamma) & Cos(\gamma)Sin(\alpha)Sin(\beta) - Cos(\alpha)Sin(\gamma) & Cos(\alpha)Cos(\gamma)Sin(\beta) + Sin(\alpha)Sin(\gamma) \\ Cos(\beta)Sin(\gamma) & Cos(\alpha)Cos(\gamma) + Sin(\alpha)Sin(\beta)Sin(\gamma) & -Cos(\gamma)Sin(\alpha) + Cos(\alpha)Sin(\beta)Sin(\gamma) \\ -Sin(\beta) & Cos(\beta)Sin(\alpha) & Cos(\alpha)Cos(\beta) \end{pmatrix} \tag{8.8}$$

Note that these definitions are using the standard mathematical conventions, i.e. the coordinate systems are right-handed and the rotations have positive signs when counter-clockwise. Finally $()_{INST} = M\,()_{ST}$, and M is now the misalignment matrix.

8.4.5 Composition of the transformations. Relation between the three matrices N, S, M

Combining the two transformations:

$$EQU \overset{S^T}{\leftarrow} ST \overset{M^T}{\leftarrow} INST \tag{8.9}$$

thus:

$$()_{EQU} = S^T M^T ()_{INST} \tag{8.10}$$

(8.10) allows to convert a source position in the instrument frame to a source position in the equatorial frame:

$$\begin{pmatrix} source \\ j \\ catalog \end{pmatrix}_{EQU} = S^T M^T \begin{pmatrix} source \\ j \end{pmatrix}_{INST} \tag{8.11}$$

Assuming $M^T = \mathbb{1}$ at launch, the source coordinates will be affected by a systematic error, and (8.11) will become:

$$\begin{pmatrix} source \\ j \\ measured \end{pmatrix}_{EQU} = S^T \begin{pmatrix} source \\ j \end{pmatrix}_{INST} \tag{8.12}$$

As defined earlier in (8.2):

$$\begin{pmatrix} source \\ j \\ measured \end{pmatrix}_{EQU} = N \begin{pmatrix} source \\ j \\ catalog \end{pmatrix}_{EQU} \tag{8.13}$$

thus equivalent to the following situation:

$$EQU \quad \overset{S^T}{\leftarrow} ST \overset{M^T}{\leftarrow} INST \tag{8.14}$$

$$N^T \uparrow$$

$$EQU \quad \overset{S^T}{\leftarrow} ST \overset{M^T=\mathbb{1}}{=} INST \tag{8.15}$$

Inserting the right hand side of (8.12) in (8.13) leads to:

$$N^T S^T \begin{pmatrix} source \\ j \end{pmatrix}_{INST} = \begin{pmatrix} source \\ j \\ catalog \end{pmatrix}_{EQU} \tag{8.16}$$

now including (8.11):

$$N^T S^T M S \begin{pmatrix} source \\ j \\ catalog \end{pmatrix}_{EQU} = \begin{pmatrix} source \\ j \\ catalog \end{pmatrix}_{EQU} \tag{8.17}$$

thus:

$$N^T S^T M S = \mathbb{1} \tag{8.18}$$

and finally:

$$N = S^T M S \tag{8.19}$$

To summarize, M is the misalignment matrix used for the correction of the source coordinates for misalignment, and S is the matrix that represents the attitude of the S/C. Both are combined in the analysis S/W (in particular in the routine DAL3AUXcalcInstrumentAttitude()), and updated each time the S/C moves to a new pointing position.

8.5 Deduction of the misalignment matrix M from the PV and calibration data

8.5.1 Use of several different sources

The simplest method to solve the problem in a unique manner is to measure a number of sources larger or equal than the number of unknowns, i.e. three. It was however not applicable in our case for the following reasons. First, during the PV phase, only two sources were clearly detected: Cyg X-1 and Cyg X-3. This was not sufficient to deduce the three Euler angles uniquely. Second, most of the *INTEGRAL* observations are made with dithering[26]. Each time the spacecraft dither to a new position, its attitude changes and the source position on the detector plane as well. While it seems to complicate a lot the computations, it could be used at our advantage. It is possible to use each new "dithered" position of the same source as if it was a different source, thus increasing dramatically the number of inputs to the problem.

8.5.2 Use of several different sources, with several pointings (dithering)

This method was used to deduce the misalignment matrices for ISGRI, JEM-X1, JEM-X2 and OMC. For PICsIT, the matrix was chosen to be the same as for ISGRI. This choice has been confirmed correct in spring 2004 by L. Foschini from the PICsIT team. In particular he has compared the results obtained with a unity matrix and concluded that the measured positions were better with the ISGRI matrix.

The sources used for the computations were the Crab (calibration data; revolutions 39 to 45) and Cyg X-1 (PV data; revolutions 12 to 21). As already mentioned in the introduction, the Crab nebula is not a point source in the X-ray range of JEM-X. One thus tried to avoid using this source. It was possible to use GRS 1915+105 (private data loaned to us by D. Hannikainen; revolution 57) instead for JEM-X2, but not for JEM-X1 as it was dormant since revolution 45, after its reactivation for the Crab calibration.

The analysis S/W is first run using a unity misalignment matrix on the selected group of pointings, and the measured ra_src and dec_src of the sources are extracted. The catalog positions of the sources are taken from the Hipparcos catalog for OMC and the ISDC reference catalog (Ebisawa et al. 2003) for the other instruments. Finally, all the corresponding S/C attitudes are extracted from the historic attitude files when available, this was not always the case, but it turned out that the error made using the snapshot attitude was small (at most $3''$, see Walter et al. 2003).

The computation of the matrix is then as follows (in order to ease the understanding, the C++ code is included in annex D; in particular, we will use the same notations).

---

[26] a controlled and systematic manoeuvre of the spacecraft which consist of several off-pointings from the target in 2 degrees steps. The hexagonal pattern is composed of 7 points while the raster 5 by 5 pattern is composed of 25 points

Using n sources, a measured **mes** vector and a catalog **cat** vector are built. They have dimension $3n$ and the following structure:

$$\begin{pmatrix} Cos(dec\_src\_\text{source1})Cos(ra\_src\_\text{source1}) \\ Cos(dec\_src\_\text{source1})Sin(ra\_src\_\text{source1}) \\ Sin(dec\_src\_\text{source1}) \\ Cos(dec\_src\_\text{source2})Cos(ra\_src\_\text{source2}) \\ \dots \end{pmatrix} \tag{8.20}$$

as well as an error **error** vector $\begin{pmatrix} \sigma_{x,1} \\ \sigma_{y,1} \\ \sigma_{z,1} \\ \dots \end{pmatrix}$ for the measured coordinates:

$$\begin{pmatrix} (Sin^2(dec\_src\_\text{source1})Cos^2(ra\_src\_\text{source1})\sigma^2_{dec\_src} + Cos^2(dec\_src\_\text{source1})Sin^2(ra\_src\_\text{source1})\sigma^2_{ra\_src})^{-1/2} \\ (Sin^2(dec\_src\_\text{source1})Sin^2(ra\_src\_\text{source1})\sigma^2_{dec\_src} + Cos^2(dec\_src\_\text{source1})Cos^2(ra\_src\_\text{source1})\sigma^2_{ra\_src})^{-1/2} \\ (Cos^2(dec\_src\_\text{source1})\sigma^2_{dec\_src})^{-1/2} \\ (Sin^2(dec\_src\_\text{source2})Cos^2(ra\_src\_\text{source2})\sigma^2_{dec\_src} + Cos^2(dec\_src\_\text{source2})Sin^2(ra\_src\_\text{source2})\sigma^2_{ra\_src})^{-1/2} \\ \dots \end{pmatrix} \tag{8.21}$$

The uncertainties on ra_src σ_{ra_src} and dec_src σ_{dec_src} were taken to be of the order of the pixel size, i.e. 0.01 degrees for ISGRI, 0.001 degrees for JEM-X and $17''$ for OMC. Finally, (8.3) is used to build the attitude matrix S and deduce its transposed S^T.

In the computation, the point is to minimize the distance between the two vectors **mes** and **cat**.

Taking all sources into account, the solutions of the problem are the parameters of the rotation which minimize the sum of all the norms of $S^T M(\alpha, \beta, \gamma)S$**cat**-**mes**.

We thus defined the following chi-square:

$$\chi^2 = \sum_{i=0}^{n} \left(\frac{\{S^T M(\alpha,\beta,\gamma) S \begin{pmatrix} cat_{3i} \\ cat_{3i+1} \\ cat_{3i+2} \end{pmatrix}\}_{3i} - mes_{3i}}{error_{3i}} \right)^2 + \left(\frac{\{S^T M(\alpha,\beta,\gamma) S \begin{pmatrix} cat_{3i} \\ cat_{3i+1} \\ cat_{3i+2} \end{pmatrix}\}_{3i+1} - mes_{3i+1}}{error_{3i+1}} \right)^2 + \left(\frac{\{S^T M(\alpha,\beta,\gamma) S \begin{pmatrix} cat_{3i} \\ cat_{3i+1} \\ cat_{3i+2} \end{pmatrix}\}_{3i+2} - mes_{3i+2}}{error_{3i+2}} \right)^2 \tag{8.22}$$

and used MINUIT called from isdcroot to minimize it, using the robust MIGRAD algorithm (James 1998). It produced α, β and γ which are introduced in (8.8) to reconstruct M.

8.5.3 Use of one single source, with several pointings (dithering)

This method was used for SPI to increase the matrix precision and is similar to the previous one. It used only one source: The Crab, measured at several S/C attitudes using hexagonal dither patterns. Basically, the equation (8.22) above applies, the sum is made on the pointings, the S matrices are different for each index i. Since with SPI the roll axis is inevitably poorly determined, we tried to fix the angle α to 0. The uncertainties on ra_src σ_{ra_src} and dec_src σ_{dec_src} were taken to be 0.05 degrees for SPI.

8.5.4 Results for OMC

Our results for OMC have been compared to the ones of A. Domingo from the OMC team. Using the IRAF package, he centered a large number of stars on the CCD boxes. He worked directly in the detector plane and thus probably reduced the projection effects. The precision of his matrix was slightly better than ours, it was thus decided to store his matrix in the archive.

It is important to note that the definition of the +roll angle used by the OMC team is clockwise while it is anti-clockwise in our (DAL3AUX) system.

The accuracy of the misalignment matrix for OMC has been estimated to be of the order of 9″ i.e. about half an OMC pixel. No differences were noticed on the border of the OMC FOV.

8.5.5 Results and tests

The six resulting matrices M are as follows.
For ISGRI:

$$\begin{pmatrix} 0.99999672 & -0.00106535 & -0.00232783 \\ 0.00106619 & 0.99999936 & 0.00036281 \\ 0.00232744 & -0.00036529 & 0.99999722 \end{pmatrix}$$

For PICsIT (same as ISGRI, by choice):

$$\begin{pmatrix} 0.99999672 & -0.00106535 & -0.00232783 \\ 0.00106619 & 0.99999936 & 0.00036281 \\ 0.00232744 & -0.00036529 & 0.99999722 \end{pmatrix}$$

For SPI:

$$\begin{pmatrix} 0.99999713 & 0.00026549 & -0.00237837 \\ -0.00026902 & 0.99999887 & -0.00147732 \\ 0.00237797 & 0.00147796 & 0.99999608 \end{pmatrix}$$

For JEM-X1:

$$\begin{pmatrix} 0.99999674 & -0.00104390 & -0.00232831 \\ 0.00104556 & 0.99999919 & 0.00071200 \\ 0.00232757 & -0.00071443 & 0.99999703 \end{pmatrix}$$

For JEM-X2:

$$\begin{pmatrix} 0.99999708 & -0.00064733 & -0.00232631 \\ 0.00064816 & 0.99999972 & 0.00035513 \\ 0.00232608 & -0.00035663 & 0.99999723 \end{pmatrix}$$

For OMC (as given by OMC team):

$$\begin{pmatrix} 0.99999870 & -0.00096954 & -0.00128844 \\ 0.00096954 & 0.99999830 & 0.00156844 \\ 0.00128841 & -0.00156844 & 0.99999794 \end{pmatrix}$$

To evaluate the number of significant digits in the matrix components, we used the uncertainty given by MIGRAD on the three angles α, β, γ. With (8.8), we have propagated the uncertainties and obtained values of the order of 10^{-7}, and thus decided to take 8 digits after the coma.

SO(3) tests

M has to be orthogonal to conserve the orthonormality of the rotated basis, i.e. the matrix has to satisfy $M^T M = \mathbb{1}$ (it can easily be shown that this imply $det\, M = 1$). Both relations are met by construction but we checked them afterward anyway and found that in all the results we discussed, this was always the case.

Test on the data

The next test is to make sure that the rotation goes in the correct direction. To do this, we apply $N^T = (S^T M S)^T$ on the **mes** vector and make sure that the result (the corrected **cor** vector) matches the **cat** values.

To give a more detailed example of the application of the method, we will detail hereafter the computation of the ISGRI matrix which was repeated in 2004.

8.6 New computation of the ISGRI matrix in 2004

Two major modifications have been included in the ISGRI software in 2003-early 2004. The first is the distance mask-detector which has been precised and the second is a new modeling of the sources during the cleaning phase, i.e. a new Point-Spread Function (PSF) has been introduced. As these changes should slightly modify the source localisation, a new misalignment matrix for ISGRI was computed in June 2004.

We used the software prepared for the OSA 4.0 release, i.e. ibis_science_analysis 7.2 which includes ii_skyimage 3.8.1, with IC_TREE 5.9. We analysed the data COR to IMA in the 15–100 keV energy range using a unity matrix. The following data were analysed: 366 science windows (scw) revolutions 12–21 (Cygnus X-1) and 449 scws, revolutions 39–45 (Crab). The historic attitude data were used for all scws.

The modeling is indeed better as much less sources were fitted (only one) when compared to the previous computation. We thus used the coordinates found in isgri_sky_res.fits. The results are shown in Fig. 8.4.

The method described above was then used to deduce the misalignment matrix; the two sets of data - Cygnus X-1 and Crab - were used to minimize the χ^2. The angles found are: $\alpha = -0.00044487 \pm 0.00006120$, $\beta = -0.00231001 \pm 0.00000531$, $\gamma = 0.00102758 \pm 0.00000482$ and can be compared with the angles found in 2003: $\alpha = -0.00036529 \pm 0.00006923$, $\beta = -0.00232744 \pm 0.00000770$, $\gamma = 0.00106620 \pm 0.00000615$. The matrix found is:

$$\begin{pmatrix} 0.99999680 & -0.00102655 & -0.00231046 \\ 0.00102757 & 0.99999937 & 0.00044249 \\ 0.00231000 & -0.00044486 & 0.99999723 \end{pmatrix} \tag{8.23}$$

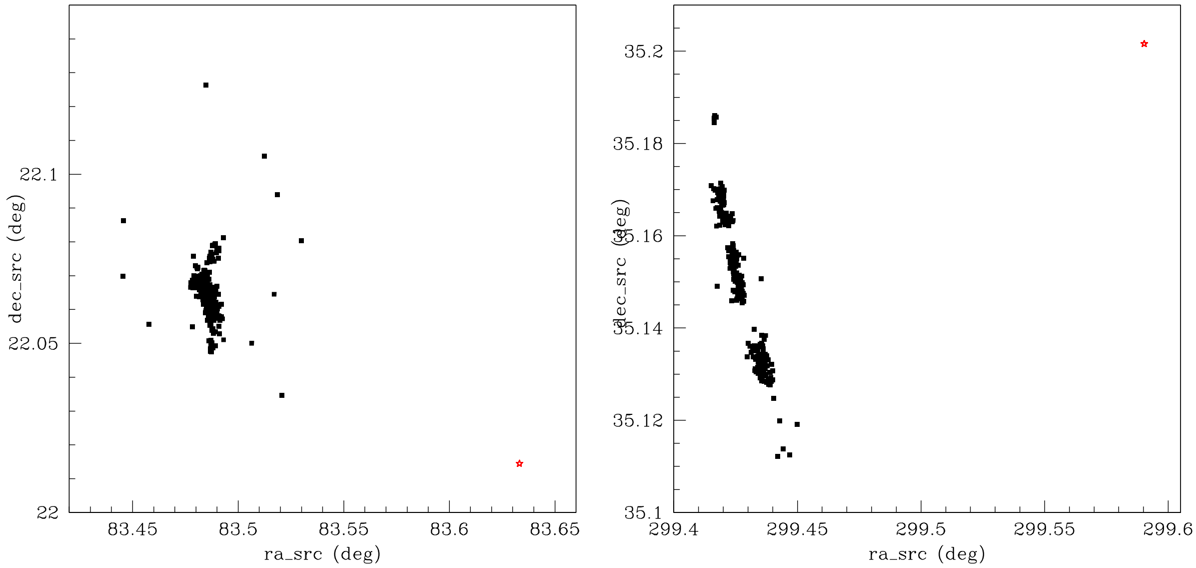

Figure *8.4: Position of Cygnus X-1 (left panel) and Crab (right panel) after analysis with a unity misalignment matrix. The catalog position is indicated by a red star.*

and will be active starting the 29th of June 2004.

The orthogonality test $M^T M$ yielded a matrix very close to unity, with off-diagonal terms of the order of 10^{-20}. We have applied $(S^T M S)^T$ on the **mes** vector and compared it to the catalog position. The correction after minimization is shown in Fig. 8.5.

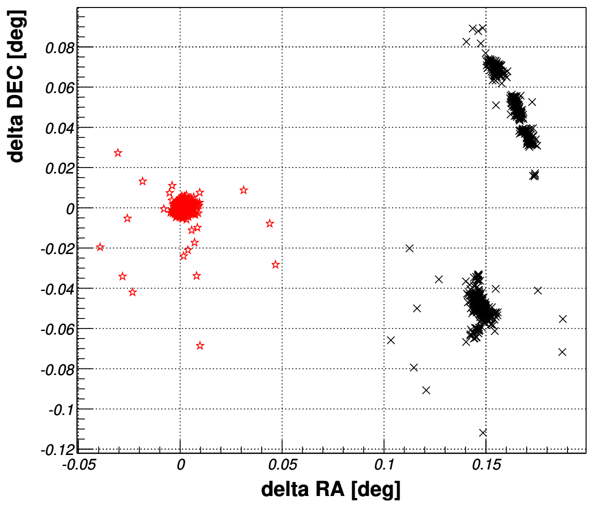

Figure *8.5: Deviation from the catalog position (0,0) for Cygnus X-1 and Crab, corrected with the 2004 ISGRI misalignment matrix (in red). In black, deviations given by the analysis S/W using a unity matrix.*

The matrix was then tested on Crab data, 427 scws, revolutions 39–45, i.e. the S/W was run using the new misalignment matrix. The deviations from the catalog position are shown in Fig. 8.6, right panel.

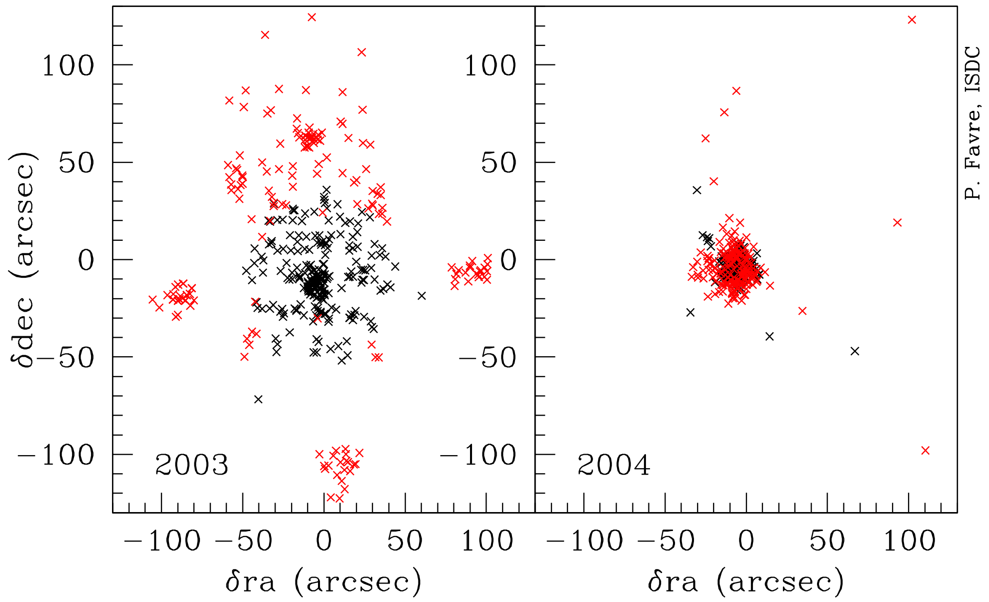

Figure *8.6: Results obtained with the analysis software including the 2004 ISGRI misalignment matrix. The deviations of the Crab positions with respect to the catalog position obtained in 2003 (left panel) are compared to the results obtained in 2004 (right panel). The black points include observations with source offset between 0 and 5 degrees while the red points include offset between 5 and 15 degrees.*

The cluster of points obtained in 2004 is better centered on the (0,0) position with respect to the 2003 results. Its size has been reduced as well. The residual offsets, computed with:

$$of_i = (\{Cos(dec\_cat_i)(ra\_src_i - ra\_cat_i)\}^2 + \{dec\_src_i - dec\_cat_i\}^2)^{-1/2} \qquad (8.24)$$

is now almost independent of the off-axis angle:

$$a_i = (\{Cos(dec\_cat_i)(ra\_scx_i - ra\_cat_i)\}^2 + \{dec\_scx_i - dec\_cat_i\}^2)^{-1/2} \qquad (8.25)$$

see Fig. 8.7.

8.6.1 Residual offsets for JEM-X

The residual offsets computed with (8.24) and (8.25) on the 2003 data, as a function of the off-axis angle are presented in Fig. 8.8.

8.7 Discussion

The misalignments are similar in direction and amplitude and dominated by an offset of $9'$, thus suggesting that the star trackers are responsible for a large part in the systematics.

Once the systematics corrected, the on-axis residuals are quite small (Table 8.1).

Fig. 8.9 summarizes the results for the high energy instruments. It shows the distributions of the deviations from the catalog positions for the Crab (ISGRI, SPI, JEM-X1) and Cyg X-1

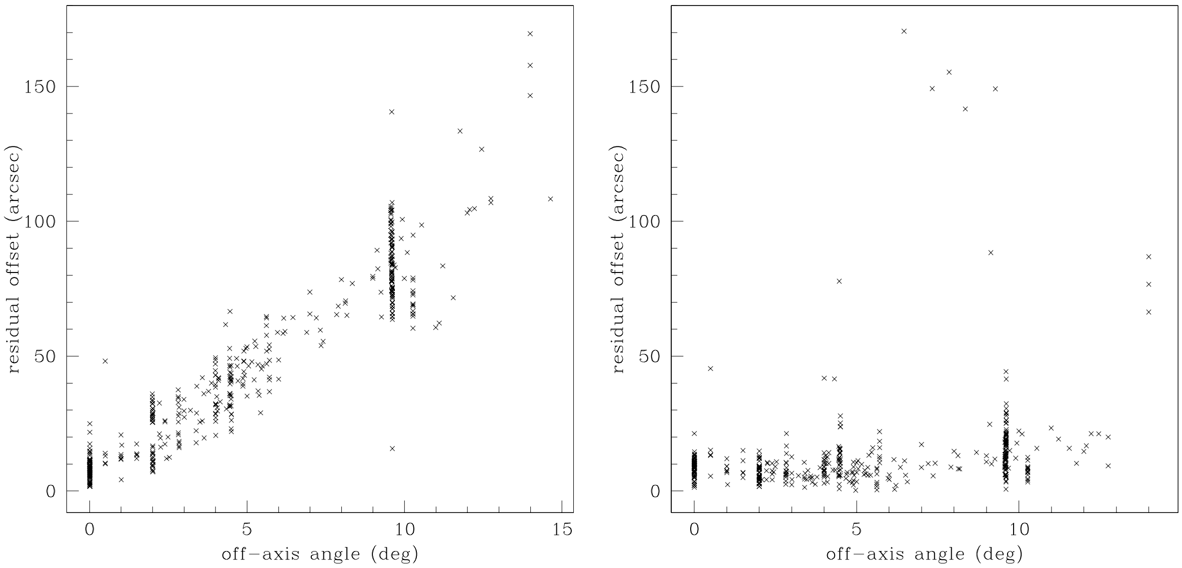

Figure *8.7: Residual offsets as a function of the off-axis angle. Results obtained in 2003 (left panel) and 2004 (right panel).*

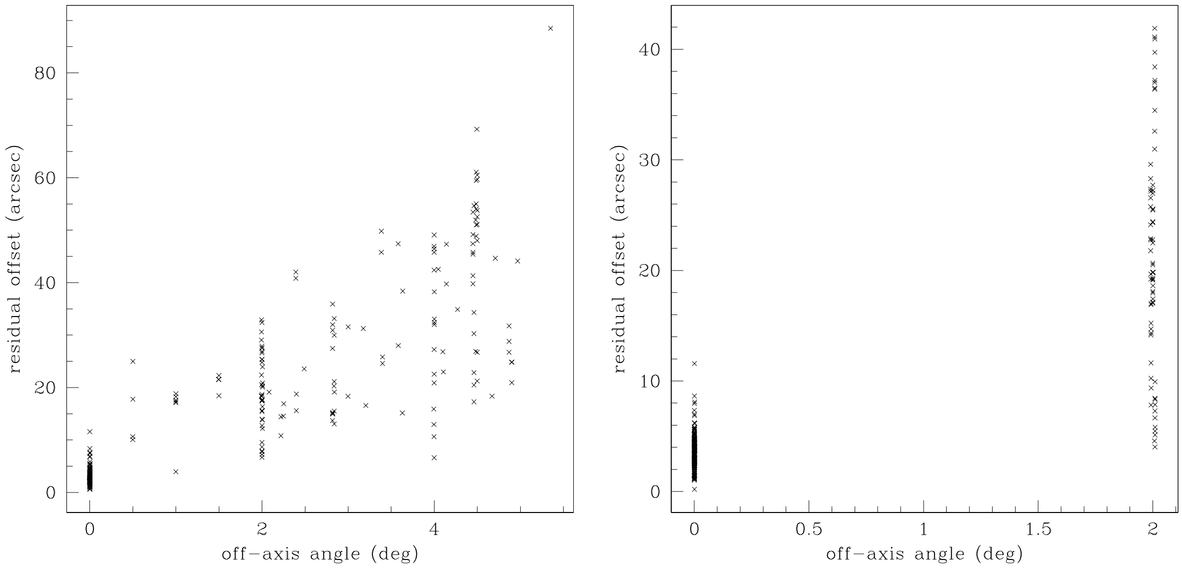

Figure *8.8: Residual offsets as a function of the off-axis angle. Results obtained in 2003 for JEM-X1 on the Crab (left panel) and for JEM-X2 on Cygnus X-1 (right panel).*

for JEM-X2, once the misalignment matrices were used in the analysis. For SPI, each point in the figure represents a group of 10 dither pointings.

Using the residual offsets vs the off-axis angle plots, we deduced the residual error on average (roughly at the border of the FCFOV) and on the edge of the PCFOV, see Table 8.2.

Whenever possible, we tried to minimize the intrinsic uncertainties prior to the compu-

Table 8.1: The value of the residual offset (1 sigma) after analysis of Crab data with the misalignment matrices. The (expected) spatial resolution and pixel size are given to ease comparison.

Instrument	Residuals on-axis	Matrix date	Spatial res.	Pixel size
ISGRI 2003	$15''$	17-07-2003	$12'$	$4.6'$
ISGRI 2004	$10''$	28-06-2004	$12'$	$4.6'$
PICsIT	$< 5'$	17-07-2003	$12'$	$9.6'$
SPI	$\sim 40''$	17-07-2003	$30'$	$2.3'$
JEM-X1	$4''$	17-07-2003	$1'$	$4'$
JEM-X2	$< 4''$	17-07-2003	$1'$	$4'$

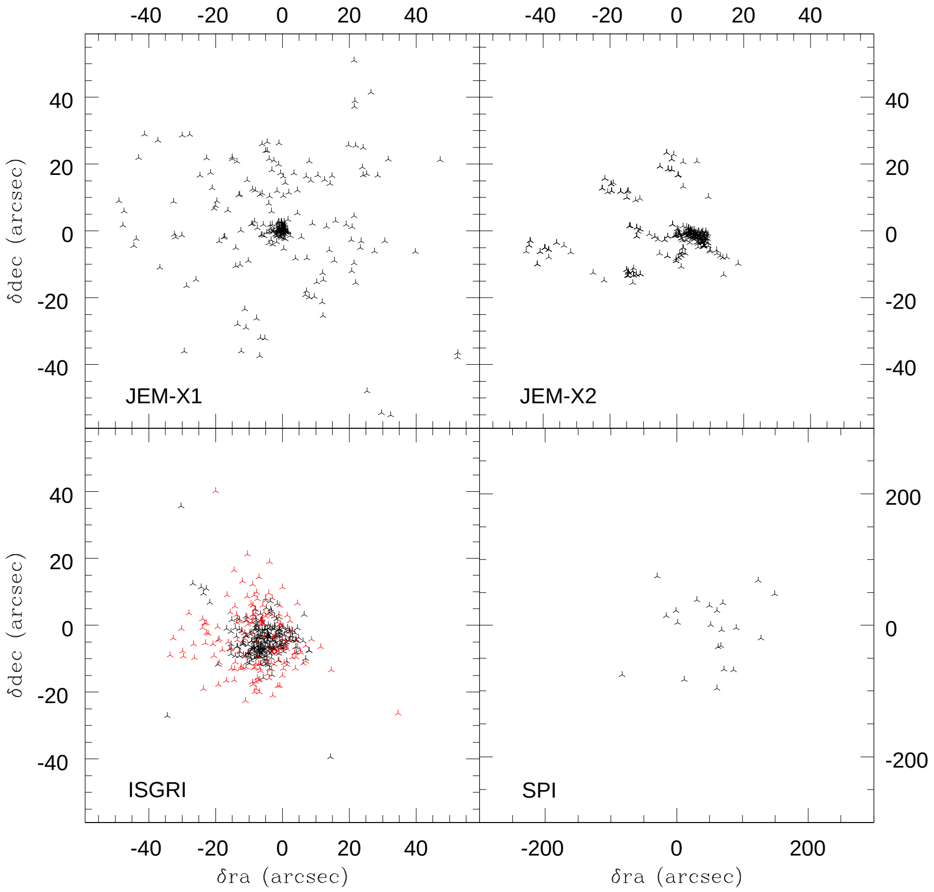

Figure *8.9: Distributions of the deviations from the catalog positions, for the Crab (ISGRI, SPI, JEM-X1) and Cyg X-1 for JEM-X2, once the misalignment matrices were used in the analysis.*

tation, e.g. by using groups of pointings in SPI. For JEM-X, we selected only the pointings which had an attitude stable within $2.5''$. The remaining limitations in the precision of the

Table 8.2: Residual offset (radius) on the positions of the Crab corrected for misalignment.

Instrument	Position residuals		
	On-axis	Mean	Edge of the PCFOV
ISGRI 2003	$15''$	$40''$	$140''$
ISGRI 2004	$10''$	$18''$	$< 40''$
PICsIT 2003	$< 5'$		$10 - 12'$
SPI		$40''$	
JEM-X1	$4''$	$18''$	$50''$
JEM-X2	$4''$	$18''$	$50''$

matrices are due to the fact that snapshot attitude was used for JEM-X and SPI, and that the Crab is not a point source for JEM-X1. Increasing the number of (different) sources taken in the computation could improve the results as well.

We have seen that a new PSF modeling has improved severely the ISGRI results, one could hope that similar improvement could be made for SPI as well.

8.8 Localisation of Gamma-ray bursters

The 2004 results for ISGRI should improve the accuracy on the position of Gamma-ray bursts (GRB) detected with IBAS (Mereghetti et al. 2003a). In 2003, the error was smaller if the burst was located in the FCFOV, this should not be the case anymore.

The localisation of GRB was a first application of the misalignment correction. On 12 December 2002, S. Mereghetti, D. Gotz and J. Borkowski, reported the detection of GRB021219 in the field of view of ISGRI (GCN 1766). GRB021219 was the second GRB in the FOV of *INTEGRAL* (the first was GRB021125, see GCN1706) and the first detected with IBAS. The burst lasted about 4 seconds, and had a peak flux of about 10^{-7} erg cm^{-2} s^{-1} in the 25–100 keV range. The preliminary position was ra=18h50m and dec=+31deg 52m with an uncertainty of $20'$ (radius) dominated by systematics.

Since it happenened in the middle of the PV phase, the misalignment matrix computation was not ready for ISGRI due to the lack of data. The method was however completed and we could derive relatively quickly a refined position for this GRB by adapting the C++ code. Together with D. Götz from the IBAS team, we were able to bring down the uncertainty on the position to about $4'$ (see GCN1768, Fig. 8.10). Triangulation by the IPN (see GCN1771, 1772; Figs. 8.11, 8.12) allowed to reduce the size of the error box (see Fig. 8.13). Finally, the Gamma-ray data (ISGRI and SPI) were published in the special issue of A&A dedicated to *INTEGRAL* (Mereghetti et al. 2003b).

At the time of writing (2nd of August 2004), 14 GRBs have been detected in the FOV of *INTEGRAL*, 13 have been triggered with IBAS.

8.9 Technical details

The next two sections are provided to allow the ISDC staff to repeat the computations described above whenever necessary in the future.

```
TITLE:   GCN GRB OBSERVATION REPORT
NUMBER:  1768
SUBJECT: GRB021219 refined position with INTEGRAL
DATE:    02/12/19 18:07:56 GMT
FROM:    INTEGRAL Shift Ops at INTEGRAL  <shift@isdcmail.unige.ch>

D.Gotz (IASF-Milano), P.Favre (ISDC), S.Mereghetti (IASF-Milano)
and J.Borkowski (ISDC) and the INTEGRAL Science Working team
report :

Further analysis of the INTEGRAL IBIS data led to a
refined position of GRB021219  of  RA 18h 50.5m DEC 31deg 54m
(J2000) with an uncertainty of 4 arcmin.
```

Figure *8.10: GCN GRB OBSERVATION REPORT 1768.*

```
TITLE:   GCN GRB OBSERVATION REPORT
NUMBER:  1771
SUBJECT: IPN triangulation of GRB021219
DATE:    02/12/19 22:27:31 GMT
FROM:    Kevin Hurley at UCBerkeley/SSL  <khurley@sunspot.ssl.berkeley.edu>

K. Hurley and T. Cline, on behalf of the Ulysses GRB team, and

D.Gotz (IASF-Milano), P.Favre (ISDC), S.Mereghetti (IASF-Milano),
J.Borkowski (ISDC), and the INTEGRAL Science Working team,
report:

This burst (GCN 1766, 1767, 1768) was also observed by Ulysses.

Although the INTEGRAL timing is still undergoing refinement, we have
triangulated it assuming a systematic uncertainty of 100 ms, which is
supported by recent SGR observations.  The preliminary annulus is
centered  at RA, Decl(2000)= 182.935, 36.337 degrees, with radius
78.549 +/-  0.023 degrees (3 sigma ).  This annulus intersects the
INTEGRAL error circle given in GCN 1768 at two points:

          RA                                  DEC
     282.557459=18 H 50 M 13.79 S      31.832096= 31 o 49' 55"
     282.642596=18 H 50 M 34.22 S      31.932013= 31 o 55' 55"

This reduces the error box size to about 15 square arcminutes.
This annulus may be improved.  A map has been posted at
ssl.berkeley.edu/ipn3/021219.
```

Figure *8.11: GCN GRB OBSERVATION REPORT 1771.*

The six misalignment matrices are grouped in the file "inst_misalign_<time stamp>.fits". It is part of data structures with auxiliary information and is not IC data as in some other missions. The extension name of the data structure is GNRL-IROT-MOD and the repository of the FITS file is $REP_BASE_PROD/aux/adp/ref/irot.

The file includes 3 keywords and the matrices. TVALID is the observation time starting from which the misalignment matrix is valid, ST_ID is the star tracker number (1 or 2) while INSTRUMENT is the instrument name and should take the following: ISGRI, PICSIT, SPI, JMX1, JMX2, OMC. The matrices are stored in MATRIX.

The storage of the 3×3 matrices in a 6×9 array is as follows. First line: ISGRI(0,0), ISGRI(0,1), ISGRI(0,2), ISGRI(1,0), ISGRI(1,1), ISGRI(1,2), ISGRI(2,0), ISGRI(2,1), ISGRI(2,2). Second line: PICSIT(0,0), PICSIT(0,1), picsit(0,2), etc. The instruments are in this order: ISGRI, PICSIT, SPI, JMX1, JMX2, OMC.

```
TITLE:   GCN GRB OBSERVATION REPORT
NUMBER:  1772
SUBJECT: IPN triangulation of GRB021219 - CORRECTION
DATE:    02/12/19 22:46:36 GMT
FROM:    Kevin Hurley at UCBerkeley/SSL  <khurley@sunspot.ssl.berkeley.edu>

K. Hurley and T. Cline, on behalf of the Ulysses GRB team, and

D.Gotz (IASF-Milano), P.Favre (ISDC), S. Mereghetti (IASF-Milano),
J. Borkowski (ISDC), and the INTEGRAL Science Working team,
report:

The IPN  annulus actually intersects the INTEGRAL error circle given in
GCN 1768 at four points, not two:

          RA                                 DEC
     282.572616=18 h 50 m 17 s       31.849899= 31 o  50 '   59 "
     282.664692=18 h 50 m 39 s       31.957916= 31 o  57 '   28 "
     282.546093=18 h 50 m 11 s       31.898856= 31 o  53 '   55 "
     282.601577=18 h 50 m 24 s       31.963983= 31 o  57 '   50 "

Thus the agreement between the annulus and the error circle is
improved, but the error box size increases to about 22 square
arcminutes.  A revised map has been posted at
ssl.berkeley.edu/ipn3/021219.
```

Figure *8.12: GCN GRB OBSERVATION REPORT 1772.*

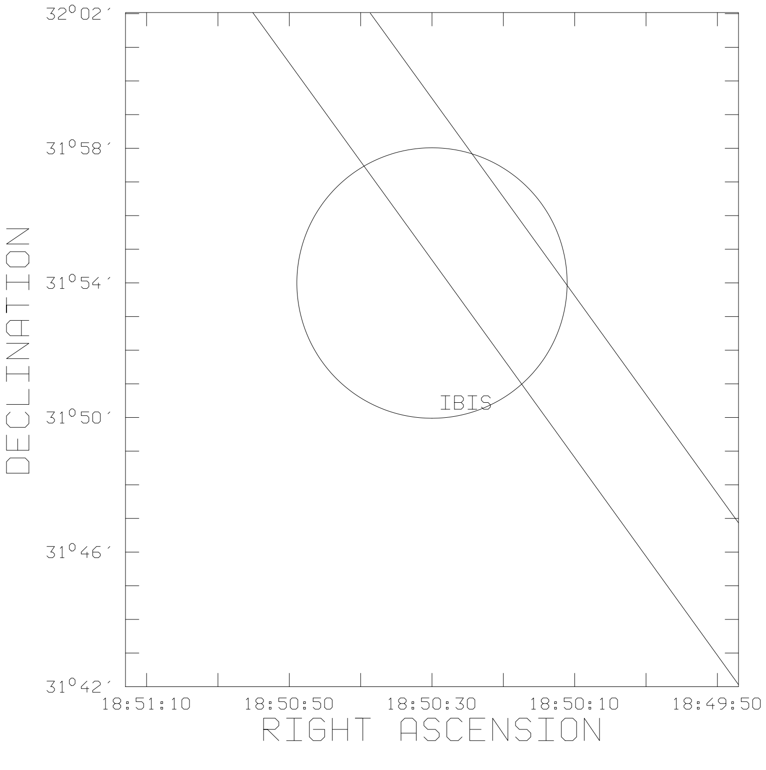

Figure *8.13: IPN map for the localisation of GRB021219.*

The matrices are used as well by ISOC for the planning of the observations.

8.10 Cookbook

The following commands are needed in order to force the S/W to use a particular matrix instead of the official one, for computation and testing purposes.

```
cd $REP_BASE_PROD
rm aux
mkdir aux
cd aux
ln -s /isdc/arc/rev_1/aux/org
mkdir adp
cd adp
foreach file (/isdc/arc/rev_1/aux/adp/0*)
ln -s $file
end
mkdir ref
cd ref
ln -s /isdc/arc/rev_1/aux/adp/ref/crst
ln -s /isdc/arc/rev_1/aux/adp/ref/de200
ln -s /isdc/arc/rev_1/aux/adp/ref/leap
ln -s /isdc/arc/rev_1/aux/adp/ref/revno
mkdir irot
cd irot
copy the modified (or unity) matrix here

cd ../../../../
```

Steps to derive a new matrix

1. set the latest OSA environment;
2. set a unity matrix and change its timestamp i.e. save it under "inst_misalign_<date of today>.fits"; the best is to copy the latest file from the archive and modify it, this would avoid template problems;
3. rebuild the auxiliary tree as explained a few lines above;
4. select the pointings which will be used for the computation;
5. run the S/W on the selected pointings;
6. get the measured ra_src and dec_src; e.g. for ISGRI get RA_FIN and DEC_FIN from all the isgri_sky_res.fits files. It is useful to save as well the corresponding scw number;
7. get the attitude data, e.g. ra_scx, dec_scx, ra_scz, dec_scz from swg_idx_ibis.fits;
8. using the scw number, make sure the correct attitude data corresponds to each ra_src and dec_src;
9. fill an ascii file (called "source" in annex C)with the following columns (in this order): ra_cat, dec_cat, ra_mes, dec_mes, ra_scx, dec_scx, ra_scz, dec_scz;

10. modify the "numlines" variable in the file misfit.cpp, adapt sigma_ra, sigma_dec, they can be adjusted by checking "sigma on coordinate";

11. run isdcroot.

To run isdcroot:

```
source /isdc/scripts/login
isdcroot
.L misfit.cpp
misfit()
```

Finally, a few checks are needed: the matrix should have passed the orthogonality tests and have been correctly copied and at the correct location in the fits file. OSA should be run on a set of data to verify its accuracy.

Bibliography

Arfken, G., 1985, Mathematical Methods for Physicists, Academic Press, 198
Brandt, S., Budtz-Jorgensen, C., Lund, N., et al. 2003a, A&A, 411, L433
Brandt, S., Budtz-Jorgensen, C., Lund, N., et al. 2003b, A&A, 411, L243
Courvoisier, T. J.-L., Walter, R., Beckmann, V., et al. 2003, A&A, 411, L53
DAL3 Auxiliary User Manual, 2004, http://isdc.unige.ch/index.cgi?Software+downloads
Ebisawa, K., Bourban, G., Bodaghee, A. et al., 2003, A&A, 411, L59
James, F. 1998, CERN Program Library Long Writeup D506, MINUIT reference manual
Mereghetti, S., Gotz, D., Borkowski, J. et al., 2003a, A&A, 411, L291
Mereghetti, S., Gotz, D., Beckmann, V. et al., 2003b, A&A, 411, L311
Pelling, R.M., Paciesas, W.S., Peterson, L.E., et al. 1987, ApJ, 319, 416
Strang, G., 1988, Linear Algebra and its Applications, Harcourt Brace & Company
Walter, R., Favre, P., Dubath, P., et al. 2003, A&A, 411, L25

A&A 411, L25–L29 (2003)
DOI: 10.1051/0004-6361:20031306

Astronomy & Astrophysics

INTEGRAL timing and localization performance

R. Walter[1,2], P. Favre[1,2], P. Dubath[1,2], A. Domingo[3], G. Gienger[4], W. Hermsen[5], J. Pineiro[4], L. Kuiper[5], M. Schmidt[4], G. Skinner[6], M. Tuttlebee[4], G. Ziegler[4], and T. J.-L. Courvoisier[1,2]

[1] *INTEGRAL* Science Data Centre, Chemin d'Écogia 16, 1290 Versoix, Switzerland
[2] Observatoire de Genève, Chemin des Maillettes 51, 1290 Sauverny, Switzerland
[3] Laboratorio de Astrofísica Espacial y Física Fundamental, PO Box 50727, 28080 Madrid, Spain
[4] European Space Operation Center, Robert-Bosch-Str. 5, 64293 Darmstadt, Germany
[5] SRON National Institute for Space Research, Sorbonnelaan 2, 3584 CA Utrecht, The Netherlands
[6] Centre d'Étude Spatiale des Rayonnements, 9 avenue du Colonel Roche, 31028 Toulouse Cedex 4, France

Received 15 July 2003 / Accepted 26 August 2003

Abstract. In this letter we report on the accuracy of the attitude, misalignment, orbit and time correlation which are used to perform scientific analyses of the *INTEGRAL* data. The boresight attitude during science pointings has an accuracy of 3 arcsec. At the center of the field, the misalignments have been calibrated leading to a location accuracy of 4 to 40 arcsec for the different instruments. The spacecraft position is known within 10 m. The relative timing between instruments could be reconstructed within 10 μs and the absolute timing within 40 μs.

Key words. instrumentation: miscellaneous – methods: data analysis – gamma rays: observations – space vehicles

1. Introduction

The timing and localization accuracies obtained from *INTEGRAL* observations depend on both the instrument performances (Ubertini et al. 2003; Vedrenne et al. 2003; Lund et al. 2003; Mas-Hesse et al. 2003) and on the quality of a set of auxiliary data. Here we present (1) the accuracy of those auxiliary data and (2) the overall performance figures. The accuracy of the star tracker boresight attitude is discussed in Sect. 2, the instrument misalignment when compared to the boresight and the imaging performance in Sect. 3, the position of the spacecraft on its orbit in Sect. 4, and the absolute timing in Sect. 5. The measured accuracies meet the requirements that were defined prior to launch.

2. Star tracker boresight attitude

The *INTEGRAL* Attitude and Orbit Control Subsystem provides the necessary functionality to control the spacecraft orientation during slews and stable pointing phases, in the so-called Inertial Pointing and Slew mode. In this mode, a CCD star tracker is used to control the pitch and yaw attitude of the spacecraft while a fine sun sensor is used to control the roll attitude around the telescope boresight. Data from the star tracker and the fine sun sensor are also used for on-ground attitude reconstruction. The *INTEGRAL* spacecraft boresight is defined by the optical axis of the operational star tracker, which in-turn is defined by the CCD reference system of the star tracker. The X–axis is the optical axis of the operational star tracker, the Z–axis points perpendicular to the solar panels towards the Sun. There are two star trackers on *INTEGRAL* and since launch only star tracker A has been used.

The star tracker is able to track up to 5 stars continuously with a full accuracy (i.e. a sub-pixel resolution of 0.245 arcsec compared to a pixel dimension of about 40 arcsec) and to produce a map of the stars in the field of view. The mapping mode is used after each slew and reaction wheel bias when the attitude is not precisely known. During a pointing the first star encountered during the mapping is tracked continuously and used as the guide star.

The position, magnitude and status of the tracked star and the raw fine sun sensor outputs, are processed to construct the measured unit vectors to the stars in the star tracker CCD coordinate system. Note that the alignments of the fine sun sensor heads have been calibrated during the commissioning phase with respect to the star tracker CCD reference system. These measured vectors calculated twice per second along with the catalogue vectors (corrected for proper motion) are then used to provide an optimal estimate of the attitude that is converted into right ascension and declination of the X and Z axis with respect to the J2000 reference system.

During dithering operations (Courvoisier et al. 2003) the typical sequence of attitude records available in the historic attitude file consists of (1) pointing records for each dither point, (2) closed loop slew and (3) settling records between dithering

Send offprint requests to: R. Walter,
e-mail: Roland.Walter@obs.unige.ch

pointings, and (4) open loop slew records for slews longer than about 4 degrees.

The *pointing* records provide attitude information during a period of stable pointing. If the difference with respect to the attitude at the start of the pointing is less than 2.5 arcsec, there will be only one entry in the attitude file. This record provides the best average attitude estimate for the duration specified. However, whenever the attitude varies by more than 2.5 arcsec as is the case during a reaction wheel bias manoeuvre, new records are created every 2 s. The accuracy during stable pointings in nominal conditions is about 3 arcsec (1σ). During science pointings (with a typical duration of 30 min), the maximum attitude deviation is less than 3 arcsec in 75% of the cases and less than 7 arcsec in any case for all star tracker axis.

The *closed loop slew* records, generated every 10 s, provide instantaneous attitude reconstruction based on the tracked guide star and the Sun. The accuracy of the attitude is slightly degraded because of the slew rate (up to 90 arcsec/s). Typically, the accuracy of the attitude record is better than 10 arcsec (2σ).

The *settling period* records provide attitude reconstruction with a time resolution of 10 s when small manoeuvres or oscillations occur at the beginning or end of a pointing. The accuracy of the attitude during the settling periods depends on the nature of the settling. After slews, the accuracy of the attitude record is better than 10 arcsec (2σ). During reaction wheel biases, when the spacecraft angular rates can be quite high, the accuracy is worse.

The *open loop slew* records provide an instantaneous attitude, which is determined based on all the mappings that are commanded during the slew. The accuracy of the attitude is slightly degraded because of the high slew rate (up to 200 arcsec/s). Typically, the accuracy of the attitude record at the mapping time is around 20 arcsec (2σ).

After a long open slew, the spacecraft attitude can be up to 1° off the targeted value. However, corrective slews are performed resulting in a final attitude that is within 1 arcsec ($1\,\sigma$) and in any case within 7 arcsec of the planned position.

3. Instruments misalignment

The instrument misalignment is defined with respect to the star tracker orientation for which the attitude solution is derived. Analysis software provided by the Integral Science Data Center (ISDC, Courvoisier et al. 2003) takes those misalignments into account to extract proper source positions.

We used pointings of the Crab Nebula (revolution 39 to 45) and of Cygnus X–1 (revolution 12 to 21) to determine the misalignment of the ISGRI, SPI and JEM–X 1 instruments. As the Crab Nebula is not a point source for JEM–X, we used the pointings of Cygnus X–1 and GRS 1915+105 (revolution 57) for JEM–X 2 (JEM–X 1 was only operated until revolution 45). For each instrument, the pointings were selected when the instrument was in a mode providing full imaging information.

For the SPI instrument, different combinations of data were tested and the best results were obtained when using Crab positions derived from analyses of large groups of pointings. The misalignment of PICSIT is assumed to be identical to that of ISGRI. For JEM–X, data were selected only when the attitude

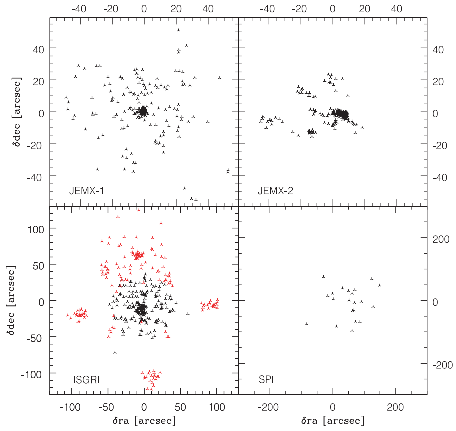

Fig. 1. Distribution of the deviations of the Crab Nebula (Cygnus X–1 for JEM–X2) positions as derived with the misalignment matrices. For SPI, each point represents a group of 10 dither pointings. For ISGRI, the cluster of points close to the origin correspond to on-axis pointings, while the other clusters are related to the source position in the field of view during the pointings used in the analysis. Pointings with the Crab Nebula >5° off axis are displayed in red.

was stable within 2.5 arcsec. The misalignment of the OMC was determined independently by comparing observed star positions to the expected ones on the CCD.

The misalignment matrix represents a rotation of the instrument frame with respect to the star tracker frame and does not depend on the attitude of the spacecraft. This rotation is performed through an Euler matrix M (e.g., Arfken 1985) such that $M\boldsymbol{str} = \boldsymbol{instr}$ where $\boldsymbol{str}$ and $\boldsymbol{instr}$ are the unity vector columns of a source direction in the star tracker respectively instrument coordinate reference system (the orientation of the coordinate systems being the same).

For each instrument and every selected pointing, we calculated the position of the source of interest assuming a unity misalignment matrix and searched for the 3 Euler angles which minimized the length of all the vectors $\boldsymbol{mes} - S^T M S \boldsymbol{cat}$ for each pointing, where $\boldsymbol{mes}$ and $\boldsymbol{cat}$ are the unity vector columns of measured position and catalog source position respectively in the star tracker coordinate reference system, and S^T is the transformation matrix from the star tracker to the equatorial coordinate frame.

The misalignment of the instruments are similar in direction and amplitude and dominated by a misalignment of 9 arcmin of the star tracker when compared to the spacecraft structure. The resulting matrices M are given in the auxiliary file `aux/adp/ref/irot/inst_misalign_20030717.fits` and are used automatically by the analysis software.

Figure 1 displays the distribution of the residual error position of the Crab Nebula (Cygnus X–1 for JEM–X 2) peak flux, once the misalignment matrices are used in the analysis. The residual error on the positions, listed in Table 1, are related to the source off-axis angle and increase from the center to the

Table 1. Residual error (radius) on the positions (at the center, on average, and at the border of the partially coded field of view) corrected for the misalignment. As the SPI analysis is based on groups of pointings, only the mean value is given.

Instrument	Position residuals		
	On-axis	Mean	Edge of the PCFOV
ISGRI	15″	40″	140″
SPI		40″	
JEM-X	4″	18″	50″

border of the partially coded field of view (PCFOV). More information will be given in Favre (2004).

Analyzing the results obtained by the OMC on board centering algorithm, the accuracy of the OMC misalignment matrix has been estimated to be better than half an OMC pixel (≈9 arcsec). No significant differences are found at the border of the OMC field of view.

4. Orbit data

The spacecraft position is measured by a differential correction technique involving an orbital model that takes into account the Earth potential, the gravitational effects of the Sun and of the Moon, the effect of the Solar radiation pressure, and the momentum control manoeuvre data. This model is constrained with ranging and Doppler measurement data providing line of sight position and velocity that are regularly collected when the satellite is visible over the Redu ground station. The accuracy of the *INTEGRAL* orbit reconstruction is normally better than 10 meters along the line of sight.

The orbital information is stored as a sequence of time ordered records. Each record is valid for few hours on average and provides the undisturbed reference Keplerian Orbit and a polynomial difference to this reference orbit to model the perturbations. The reference frame for the orbital information is the inertial mean geocentric equatorial system of J2000 (FK5). The system is centered on the Earth gravitational center with the X axis pointing towards the mean vernal equinox. The X–Y plane coincides with the mean Earth equatorial plane and the Z axis points towards the North.

5. Timing information

Measurements of the Crab pulsar indicate that absolute timing of *INTEGRAL* on-board events can be derived with an accuracy of ±40 μs. In this section we present some details of the transformation of On Board Time (OBT) into Coordinated Universal Time (UTC), and we show that at the beginning of the mission it has been affected by two kinds of unexpected delays. In addition constant instrumental delays should also be taken into account. Those delay corrections are not integrated into the analysis software distributed by the ISDC. Delays provided in the tables 2 to 4 must therefore be corrected for by the users performing precise timing analysis.

Table 2. Offset to be added to the IJD derived by the time correlation.

Period (UTC)	Offset (μs)
before 2003-05-21 07:15	964
from 2003-05-21 07:15 to 2003-07-03 14:23	867
after 2003-07-03 14:23	0

5.1. Time units and representations

The *INTEGRAL* data analysis uses essentially three time systems:

1. The Earth Reception Time (ERT), expressed in coordinated Universal Time (UTC), is defined at the reception of every telemetry frame by the ground station. The ERT is determined by atomic clocks located within each of the ground stations used by the mission. The ground stations are synchronized using the Global Positioning System. Unfortunately the synchronization was found to be affected by several problems (Sect. 5.2).
2. The Terrestrial Time (TT) is used to time tag, on-ground, products and physical events recorded within the instruments. The terrestrial time follows precisely the Atomic International Time (TAI) and does not suffer from leap seconds. In the data products terrestrial times are always formatted as double precision real in unit of *INTEGRAL* Julian Date (IJD), defined as the number of days since the 1st of January 2000 at 0h 0m 0s (TT) (IJD = JD–2 451 544.5).
3. The On Board Time (OBT) is defined by counting the number of pulses of an oscillator on board the spacecraft. All on board times are represented as 64 bit integers with a unit of 2^{-20} OBT second even if they are less precise in the telemetry. By convention, each time the on board clock is reset, the OBT is augmented by 2^{52} (this never happened at the time of writing). In FITS files, OBT are formatted as vectors of four 2-byte integers (for columns) or as 20 characters numeric string (for keywords).

5.2. Time correlation

The time correlation is the relation between IJD and the on board time (OBT). It is derived from measurements, in OBT unit, of the time at which specific telemetry frames leave the spacecraft (more specifically the leading edge of the first frame bit). Those OBT measurements are then correlated to the Earth Reception Time of the corresponding frames. Corrections for on board delays, delays within each of the ground stations and light travel time are taken into account.

The on board delays were calculated and calibrated on ground. Unfortunately, at the beginning of the mission, the on board delay was taken into account with a wrong sign in the time correlation software with the net effect that any IJD derived from an OBT should be corrected by a positive offset as listed in Table 2. This correction is not performed by the analysis software yet and needs to be added to the terrestrial time derived from the time correlation. On 2003-05-21 07:15 the telemetry rate of *INTEGRAL* was increased by 25%

Table 3. Delays observed between the various ground stations and IJD (as defined by the VILSPA 2 ground station). A positive delay indicates that for a given OBT, the IJD derived using the ground station in reference is smaller than it should be. A mean value and its uncertainty is provided for all periods during which the delays varied significantly. This means that values without reported errors are more accurate than the others.

Ground Station	Period (UTC)	Delay (μs)
ESA Redu	before 2003-02-26 14:05	-110 ± 10
ESA Redu	2003-02-26 14:05 to 05-12 15:28	-15 ± 20
ESA Redu	2003-05-12 15:28 to 05-15 15:25	-105 ± 10
ESA Redu	2003-05-15 15:25 to 05-21 15:14	0 ± 5
ESA Redu	2003-05-21 07:15 to 07-03 14:23	74 ± 5
ESA VILSPA 2	before 2003-05-21 07:15	0
ESA VILSPA 2	2003-05-21 07:15 to 07-03 14:23	73
NASA DSS–16	before 2003-05-21 07:15	42
NASA DSS–16	2003-05-21 07:15 to 07-03 14:23	34
NASA DSS–24	before 2003-04-01 12:00	−78 081
NASA DSS–24	2003-04-01 12:00 to 05-21 07:15	54
NASA DSS–24	2003-05-21 07:15 to 07-03 14:23	43
All	after 2003-07-03 14:23	0

resulting into a new correction offset. The software was corrected on 2003-07-03.

In addition, time offsets are observed at ground station handovers. This means that systematic, and sometimes variable, delays are present between the timings of the different ground station. Besides the effect of the change of telemetry rate, those problems were dominated by a miscalibration of the Goldstone DSS–24 station at the beginning of the mission, and by synchronization problems within the Redu ground station. All calibrations were corrected on 2003-07-03.

Table 3 lists the observed delays that should be added by the user to any IJD derived from an OBT to obtain an absolute time reference (this correction is not performed by the analysis software yet). The time derived from the VILSPA 2 station (except for the period from 2003-05-21 to 2003-07-03) is taken as the reference. Note however that the UTC derived from NASA ground stations leads the UTC derived from ESA ground stations by about 40 μs. For now this should be considered as a residual systematic error.

5.3. Instrument timing information

A portion of the OBT counter is made available by the spacecraft to the *INTEGRAL* instruments which are synchronized to the spacecraft at the beginning of every revolution (this synchronization involves a delay of 15 μs that is taken into account in Table 4). All instruments except the spectrometer use the same clock pulse to time tag physical measurements. Those time tags (local on board time) are transmitted in the telemetry, stored unchanged in the raw data, and converted to full OBT unit in the subsequent steps of the data processing, providing a single OBT representation for all times to the analysis software. The spectrometer camera uses its own internal oscillator to tag events. Those time tags are converted to the standard OBT using specific time synchronization information.

Table 4. Delays between the event time and the event time tag (reconstructed for SPI) for the high energy instruments. The positive delay should be added to the event OBT time tag to get the absolute event time. The delay was calibrated on ground and measured in-flight comparing *INTEGRAL* and *RXTE* Crab light curves in absolute phase.

Instrument	Delay (ground calibration) (μs)	Delay (Crab timing) (μs)
SPI	134 ± 10	138 ± 40
IBIS	111 ± 10	135 ± 40
JEM–X	185 ± 10	216 ± 40

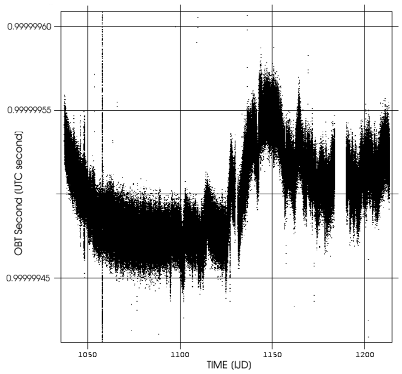

Fig. 2. OBT second corrected for thermal effects as a function of time.

The delays between the actual event times and the instrument OBT time tags were measured on ground before the launch (Alenia 2002) and are given in the first column of Table 4. These delays are also derived from flight data using contemporary *INTEGRAL* and *RXTE* observations of the Crab pulsar (Kuiper et al. 2003). For all *INTEGRAL* instruments and *RXTE*, the differences in arrival times of the first (main) Crab peak in the pulse profile in radio and X-rays are measured. The differences between the *INTEGRAL* and *RXTE* measurements, both using the Goldstone DSS–16 ground station, of the X-ray-radio delay is a measure of the instrumental delays, taking *RXTE* as the standard. For *RXTE* an X-ray-radio delay of 268 ± 30 μs was determined, consistent with the 302 ± 67 μs found by Rots et al. (2000) (see also Tennant et al. 2001). The obtained differences are also listed in Table 4. The quoted errors reflect mainly the systematic uncertainty in the radio ephemeris due to variations in the dispersion measure. The delays measured on ground and in-flight are fully consistent, and should be taken into account for any absolute timing analysis. Formally those delays should be added to the on board times before applying the time correlation.

5.4. On board clock stability

The on board clock frequency varies with the oscillator temperature. Figure 2 displays the on board clock second (measured in Atomic International Time as measured by the ground station atomic clocks), corrected for the thermal effects.

The period of the on board clock is found constant over a time scale of 6 months with an accuracy of 0.1 μs/s. The residual slow variations are not correlated to the orbital parameters nor with ground station usage, as expected. This confirms that the light travel time is properly calculated.

6. Conclusion

The mean *INTEGRAL* boresight attitude during a science pointing is known to within 3 arcsec. Attitude instability during a pointing is limited to 7 arcsec. The misalignment matrices provide on-axis source localization accuracy for bright sources better than 4 arcsec, 15 arcsec and 40 arcsec for JEM–X, ISGRI and SPI respectively. This can be considered as a systematic uncertainty on the localization accuracy. The localization is further limited for large off-axis angle and by statistical uncertainties for faint sources.

The position of the spacecraft on the line of sight is known within ±10 meters. Systematic uncertainties on the relative timing have been calibrated within 10 μs. An additional systematic uncertainty of about 40 μs should be taken into account when comparing *INTEGRAL* timing with absolute times.

Instrument misalignment matrices are integrated in the analysis software system provided by the ISDC (Off-line Scientific Analysis version 2.0). This is not yet the case for the time delays given in Tables 2 to 4. For accurate timing analysis users need to take those time delays into account themself.

References

Alenia Spazio 2002, *INTEGRAL* End-to-End Timing Test Report, INT-RP-AI-0227, European Space Agency

Arfken, G., 1985, Mathematical Methods for Physicists (Academic Press), 198

Courvoisier, T., Walter, R., Beckmann, V., et al. 2003, A&A, 411, L53

Favre, P. 2004, Ph.D. Thesis, Geneva Observatory

Kuiper, L., Hermsen, W., Walter, R., et al. 2003, A&A, 411, L31

Lund, N., Brandt, S., Budtz-Joergensen, C., et al. 2003, A&A, 411, L231

Mas-Hesse, J. M., Gimenez, A., Culhane, L., et al. 2003, A&A, 411, L261

Rots, A. H., Jahoda, K., & Lyne, A. G. 2000, HEAD, 32, 3308R

Tennant, A. F., Becker, W., Juda, M., et al. 2001, ApJ, 554, L173

Ubertini, P., Lebrun, F., Di Cocco, G., et al. 2003, A&A, 411, L131

Vedrenne, G., Roques, J.-P., Schönfelder, V., et al. 2003, A&A, 411, L63